Solar Energy Materials & Solar Cells 128 (2014) 126–130

Contents lists available at ScienceDirect

Solar Energy Materials & Solar Cells

journal homepage: www.elsevier.com/locate/solmat

Inclusion of nanometer-sized silicon crystallites in *n*-layer for open circuit voltage enhancement in amorphous silicon solar cell

Guofu Hou *, Guijun Li, Jia Fang, Changchun Wei, Xiaodan Zhang *, Ying Zhao

Institute of Photoelectronics, Tianjin Key Laboratory of Photoelectronic Thin Film Devices and Technique, Nankai University, Tianjin 300071, PR China

ARTICLE INFO

Article history:
Received 21 January 2014
Received in revised form
16 April 2014
Accepted 22 April 2014

Keywords:
Nanometer-sized Si crystallite
Quantum size-confinement effect
Amorphous silicon solar cell
Open-circuit voltage

ABSTRACT

Material properties of hydrogenated silicon *n*-layer and their impact on amorphous silicon (a-Si:H) solar cell are studied. By optimizing deposition parameters, mixed-phase *n*-layer with nanometer-sized Si crystallites embedded in a-Si:H matrix can be obtained, which demonstrates higher conductivity, lower activation energy and wider bandgap. Incorporating the mixed-phase *n*-layer into a-Si:H cell can significantly improve the open circuit voltage (V_{oc}) up to 0.95 V, which is approximately 50 mV or 100 mV higher than those cells with a-Si:H *n*-layer or microcrystalline silicon *n*-layer, respectively. The possible explanations of V_{oc} enhancement brought by the mixed-phase *n*-layer have also been discussed. Up to now, we have achieved an initial efficiency of 9.4% with high V_{oc} of 0.945 V, *FF* of 0.70 and J_{sc} of 14.2 mA/cm^2 with a-Si:H *i*-layer thickness of 300 nm and substrate temperature as high as 220 °C.

1. Introduction

Over the past decades thin-film silicon-based multi-junction solar cell, consisting of amorphous silicon (a-Si:H), amorphous silicon germanium (a-SiGe:H) and microcrystalline silicon (μc-Si:H), has been widely investigated and regarded as the most potential candidate for the next-generation thin-film photovoltaic device [1–5]. Although advanced light trapping concepts and structures have been one of the recent hot-topics and have attracted extensive interest to improve the state-of-the-art device performance [6–9], optimizing the component solar cell itself in multi-junction solar cell, on the other hand, is still the chief issue to get high conversion efficiency. As for a-Si:H top cell, how to improve the open circuit voltage (V_{oc}) is one of the most crucial issues [10–13]. Previous studies mainly focused on optimizing the absorption layers, *p*-type window layers and *p*/*i* interfaces. High hydrogen diluted intrinsic a-Si:H into the amorphous/microcrystalline phase transition region leads to V_{oc} higher than 1.0 V for pure a-Si:H solar cell [10,11]. Novel absorption layers including amorphous silicon carbide [12] and amorphous silicon oxide [13] are also reported. Much work has been performed on the *p*-type hydrogenated silicon alloy layers for the V_{oc} improvement, such as amorphous silicon carbide [14], amorphous silicon oxide [15], microcrystalline silicon carbide [16], nanocrystalline silicon [11] and nanocrystalline silicon oxide [17]. In addition, appropriate *TCO*/*p* or *p*/*i* interface treatment [18,19] and modifying the work-function of indium tin oxide (ITO) front electrode [20] can also improve V_{oc}. On the other hand, there have been fewer studies on the effect of *n*-layers and even opposite role in determining the solar cell performance was presented [21,22]. Poissant et al. reported that although μc-Si:H *n*-layer has higher conductivity and lower activation energy, it also has narrow bandgap [21]. Replacing a-Si:H *n*-layer with μc-Si:H *n*-layer in *p*–*i*–*n* solar cell could not enhance the build-in potential and thus has little benefit for the V_{oc} improvement. On the contrary, Soderstrom et al. introduced an amorphous silicon carbide *n*-layer as a buffer layer at the *n*/*i* interface in *n*–*i*–*p* solar cell, which yields high V_{oc} and *FF* on both the flat and textured substrates [22]. Another issue to be mentioned is that the available V_{oc} for *n*–*i*–*p* a-Si:H cell is higher than that for *p*–*i*–*n* cell [10,11,17,18]. This phenomena can be mainly ascribed to the fact that in *n*–*i*–*p* multi-junction solar cell the a-Si:H top cell is deposited at last; thus it can be processed at lower substrate temperature (T_s), resulting in wide bandgap for a-Si:H *i*-layer. However, a-Si:H top cell in *p*–*i*–*n* multi-junction solar cell is firstly deposited at higher T_s, which should be at least no less than T_s of a-SiGe:H or μc-Si:H cell. Therefore, how to get high V_{oc} in *p*–*i*–*n* a-Si:H top cell at higher T_s by only optimizing *n*-layer has been the topic of this paper. A wide bandgap and highly conductive Si:H layer with nanometer-sized Si crystallites (Si NCs) embedded in a-Si:H matrix was firstly fabricated. Then the opto-electronic and micro-structural properties and impact on the a-Si:H solar cell performance were investigated.

* Corresponding authors.
E-mail addresses: gfhou@nankai.edu.cn (G. Hou), xdzhang@nankai.edu.cn (X. Zhang).

http://dx.doi.org/10.1016/j.solmat.2014.04.021
0927-0248/

2. Experimental details

Amorphous silicon based thin films and solar cells were deposited using a plasma enhanced chemical vapor deposition (PECVD) process in an ultrahigh-vacuum, multi-chamber, cluster-tool system. Mixtures of PH_3, SiH_4 and H_2 were used for the fabrication of *n*-type Si:H layers deposited with silane concentration ($SC=SiH_4/[SiH_4+H_2]$) from 2% to 9%, working pressure of 0.7 Torr, substrate temperature of 150 °C and RF (13.56 MHz) power of 10 W. Eagle2000 glass substrates were used for micro-structural and opto-electronic characterization of Si:H layers. Asahi SnO_2:F substrates were used as the front electrodes for a-Si:H solar cells with configuration of glass/SiO_2:F/*p*-proto-Si:H/*i*-a-Si:H/*n*-Si:H/Al. The parallel conductivity was measured with coplanar electrode structure, while activation energy (E_a) was calculated from the temperature dependence of conductivity. The absorbance and reflectance spectra were measured with a Varian Cary 5000 UV–vis–NIR spectrophotometer. The optical bandgap (E_g) was calculated using Tauc's equation [23]

$$\alpha h\nu = A(h\nu - E_g)^n$$

where α is the absorption coefficient, h is Plank's constant, ν is the transmission frequency, and A is a constant. As for c-Si with indirect bandgap the exponent n value is 2, while it is 0.5 for a-Si:H with direct bandgap. For micro-structural characterization Raman scattering spectroscopy and high-resolution transmission electron microscopy (HR-TEM) were used. Raman scattering was measured on a glass substrate by a Renishaw RM2000 microscope with 488 nm excitation wavelength. HR-TEM was performed using Philips Tecnai G^2F20. Current–voltage characteristics and spectral response were measured with a Wacom solar simulator (WXS-156S-L2, AM1.5GMM) and a quantum efficiency system (QEX10, PV Measurement), respectively.

3. Results

3.1. Opto-electrical properties and micro-structural characterization of Si:H n-layers

By fine tuning the deposition parameters, especially the silane concentration ($SC=SiH_4/[SiH_4+H_2]$), a series of *n*-type Si:H layers were fabricated. Raman spectra of these layers shown in Fig. 1 could be deconvoluted into three Gaussian components: the crystalline part I_c (520 cm^{-1}), amorphous part I_a (480 cm^{-1}), and an intermediated interfacial part I_m (500 cm^{-1}). The crystalline fraction (X_c) was then calculated from $X_c=(I_m+I_c)/(I_a+I_m+I_c)$ [24], and the average crystallite size (D) was deduced from the relationship between the Raman red-shift according to the bond polarizability model developed by Zi et al. [25]. Opto-electronic and micro-structural properties including bandgap (E_g), conductivity (σ), activation energy (E_a), crystalline fraction and crystallite size are presented in Table 1. For the mixed-phase materials in Fig. 1 Tauc's equation is not strictly valid for the exact estimation of the band gap [26,27]. Here considering an approximation of indirect bandgap with $n=2$, Tauc's equation was just used to estimate an approximate band gap of such mixed-phase materials [27]. For samples a and b obvious peaks at 520 cm^{-1} as well as high X_c and larger crystallite size indicate a highly crystallized character. These two samples demonstrate higher conductivities and lower activation energies, but narrow bandgaps. A wide scattering band around 480 cm^{-1} indicates a fully amorphous nature for sample f and it has highest activation energy, lowest conductivity and intermediate bandgap. For samples c, d and e Gaussian function deconvoluted Raman spectra reveal a mixed-phase structure including crystalline silicon and amorphous silicon. Although samples c, d and e have relative lower X_c (from 10% to 30%) than samples a and b, they demonstrate similar high conductivities and lower activation energies. In addition samples c, d and e have much wider bandgaps, while comparing the highly crystallized films (samples a and b) or the fully amorphous layer (sample f).

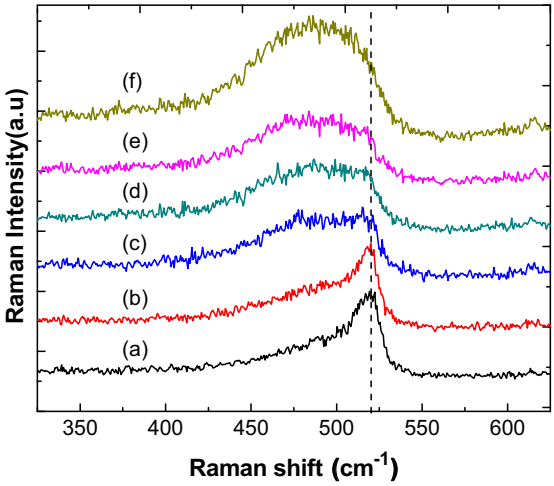

Fig. 1. Raman spectra of *n*-type Si:H layers with thickness of 30 nm on glass substrates.

Table 1
Opto-electronic and micro-structural properties of different *n*-type Si:H layers with thickness of 30 nm on glass substrates.

Sample no.	E_a (meV)	σ (S/cm)	E_g (eV)	X_c (%)	D (nm)
a	26	5.63	1.3	50	10
b	28	5.31	1.38	42	8
c	29	2.66	2.05	22	2.6
d	35	0.94	2.03	15	1.4
e	50	0.053	2.05	12	0.9
f	195	0.0042	1.83	0	0

HR-TEM characterization was carried out to acquire more detailed microstructure of the above *n*-type Si:H layers. In order to simulate a more realistic structure a 5 nm thick intrinsic a-Si:H layer was first deposited on the copper TEM grids and then a 20 nm thick *n*-type Si:H layer was grown. This hybrid structure was designed to correspond to the standard *i*/*n* interface in *p*–*i*–*n* a-Si:H solar cell. Samples with hybrid structures were named to be B, D and F, of which the 20 nm thick *n*-type Si:H layer was fabricated with identical deposition parameters as that of samples b, d and f in Table 1, respectively. Fig. 2(a) shows the HR-TEM image of sample B, in which Si-NCs with diameter around 10 nm or even larger could be found. The Si-NC density is high and these Si-NCs are connected to each other, which indicate a highly crystallized nature. As for sample D shown in Fig. 2(b) a mixed-phase structure could be revealed with Si-NCs with smaller diameters from 2 nm to 5 nm embedded a-Si:H matrix. The Si-NC density is low and most of Si-NCs exist in isolated states, which show a strong quantum size-confinement effect. Selected area diffraction patterns for samples B and D, inset of Fig. 2(a) and (b), respectively, also indicate different crystalline fractions. For a-Si:H sample F no obvious crystal grain exists, as shown in Fig. 2 (c). The HR-TEM images in Fig. 2 provide direct evidence and further confirm the above-mentioned analysis based on the Raman spectra.

3.2. Effect on a-Si:H solar cell performance

Applying *n*-type Si:H films presented in Table 1 as *n*-layers, a series of a-Si:H solar cells have been fabricated with the same

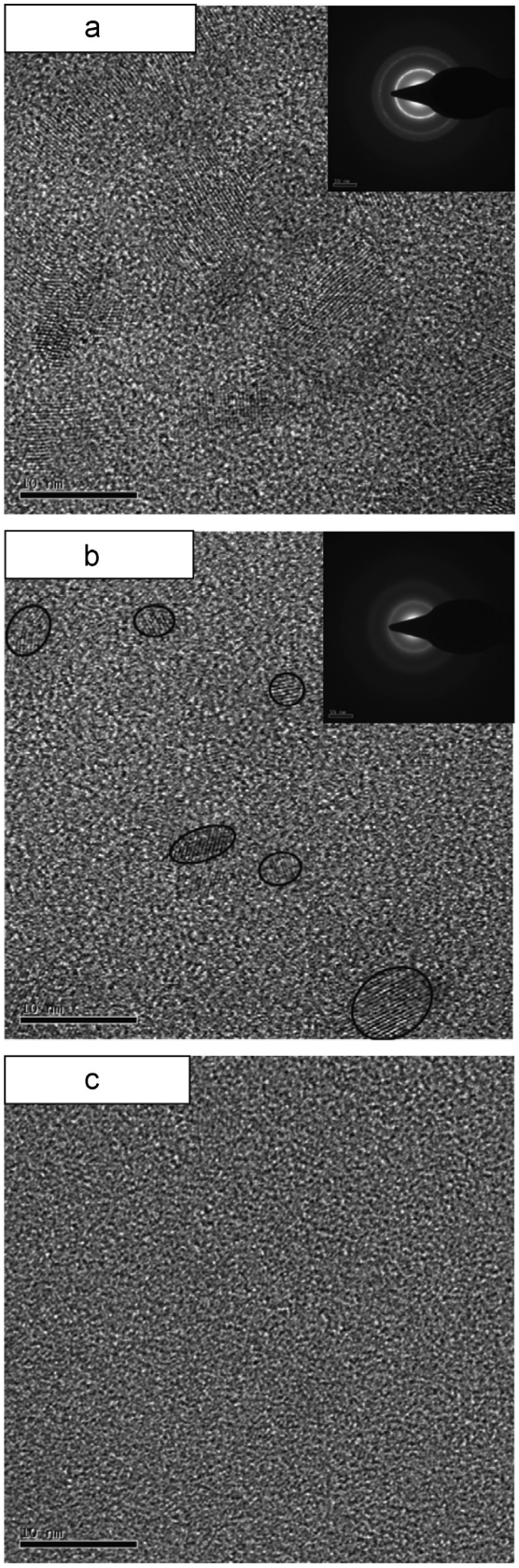

Fig. 2. High-resolution TEM images of sample B, D and F. Selected area diffraction patterns for sample B and D are also shown in the inset of (a) and (b), respectively.

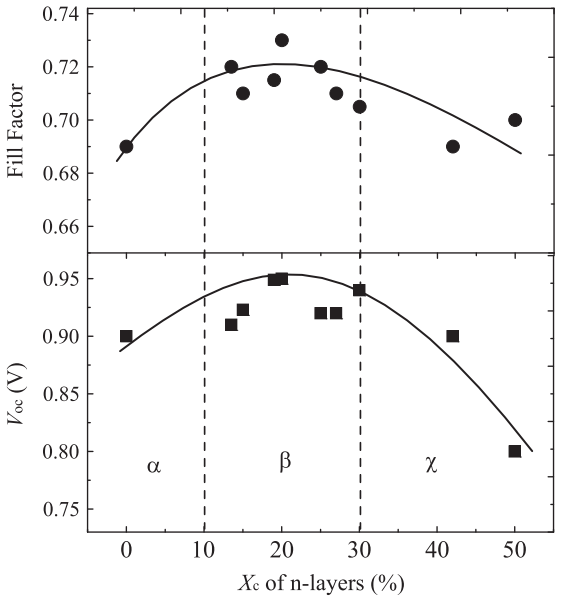

Fig. 3. V_{oc} and *FF* of a-Si:H solar cells as a function of X_c of *n*-layers.

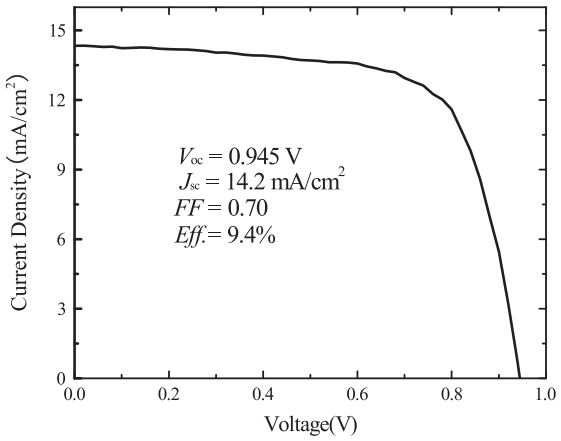

Fig. 4. *J–V* curve of the best a-Si:H solar cell with mixed-phase nc-Si:H *n*-layer.

p- and *i*-layers. V_{oc} and *FF* as a function of X_c of *n*-layers are plotted in Fig. 3, which can be divided into three regions named α, β and χ. In region α X_c is in the range from 0% to 10%; amorphous structure is dominated in these *n*-layers and V_{oc} is around 0.90 V. In region β X_c of *n*-layers range from 10% to 30%, which correspond to mixed-phase nc-Si:H with nanometer-sized silicon crystallites embedded in a-Si:H matrix as that in Table 1 and Fig. 2. Both V_{oc} and *FF* can be significantly improved. For those solar cells with high X_c *n*-layers in region χ significant V_{oc} decrease can be observed.

Typical V_{oc} of a-Si:H solar cells in region β with nc-Si:H *n*-layers are around 0.95 V, which is approximately 50 mV or 100 mV higher than those cells with a-Si:H *n*-layer or microcrystalline silicon *n*-layer, respectively. The best cell, we have achieved up to now, has V_{oc}=0.945 V (*FF*=0.70, J_{sc}=14.2 mA/cm^2 and η=9.4%) with 300 nm *i*-layer, as shown in Fig. 4. What should be mentioned here is that the substrate temperature for a-Si:H intrinsic layer is as high as 220 °C. Thus this high V_{oc} a-Si:H solar cell could be used as the top cell in multi-junction spectrum-splitting solar cell.

4. Discussion

Above results indicate that V_{oc} of a-Si:H solar cell can be remarkably improved by fine tuning the opto-electronic and micro-structural properties of Si:H *n*-layer into a mixed-phase

structure with Si-NCs embedded in a-Si:H matrix. The mixed-phase nc-Si:H *n*-layer was deposited just above the phase transition region from amorphous silicon to microcrystalline silicon. It has not only lower activation energy, higher X_c and higher conductivity, but also wider bandgap. The conductivities presented in Table 1 are measured with coplanar electrode structures, where the carriers transport takes place in the lateral direction. However, in real solar cells, the carrier transport takes place in the vertical direction. It has been proved that for mixed-phase material the conductivity in the vertical direction is much higher than that in the lateral direction [28,29]. Thus the vertical conductivities for samples c, d and e will be much higher than those values presented in Table 1. Since a-Si:H solar cells in Fig. 3 were prepared with the same *p*- and *i*-layers, the higher conductivities and lower activation energies of nc-Si:H *n*-layers should lead to an increase in the built-in field in the devices, which is favorable for V_{oc} enhancement. In fact when high X_c *n*-layers are used V_{oc} of a-Si:H solar cells are even lower than those cells with fully a-Si:H *n*-layers, which is similar with the results in Ref. [21].

In addition, *n*-layers of those *p–i–n* solar cells in Fig. 3 are directly deposited on a-Si:H *i*-layers without any *i*/*n* treatment or buffer layers. For mixed-phase nc-Si:H *n*-layers nonhomogeneous growth along the deposition direction is inevitable. An amorphous incubation layer will form in the initial deposition stage, until microcrystalline growth sets in. The structural evolution is usually believed to be harmful for device performance enhancement of μc-Si:H solar cells [30,31]. However, for the mixed-phase nc-Si:H *n*-layers the structural evolution naturally leads to a graded buffer layer between a-Si:H *i*-layer and nc-Si:H *n*-layer. The microcrystallite evolves with thickness and the top part of the *n*-layer in the *p–i–n* configuration may assist in making good electrical contact with the back contact. Overall, these results indicate potential benefit for the carrier transport and collection and then V_{oc} enhancement.

Compared with the results reported in the literature [22], the mixed-phase nc-Si:H *n*-layer also has relatively wider bandgap, which can diminish optical loss in the *n*-layer and the band alignment will be favorable for the V_{oc} improvement. The wider bandgap can be mainly ascribed to the quantum size-confinement effect [32,33] because of the isolated Si-NCs with diameters from 2 nm to 5 nm confirmed by HR-TEM measurement. On the other hand, the hydrogen-induced bandgap broadening is also reasonable and inevitable [34,35] due to the fact that most part of the mixed-phase silicon films is amorphous tissues. For the nc-Si:H *n*-layers, we suppose that they are distributed between the valence band and the conduction band, which creates a barrier for the holes and the electrons in the valence and conduction bands, respectively. The blocking barrier in the valence band helps to repel the holes from the defective interface area and reduces retro-diffusion of the holes in the *n*-layer. Hence, the nc-Si:H *n*-layer enhances the collection of the charge carriers and leads to V_{oc} improvement.

5. Conclusions

We have developed a mixed-phase nc-Si:H *n*-layer and successfully incorporated it into a-Si:H based solar cell. For the mixed-phase nc-Si:H *n*-layer, its higher conductivity and lower activation energy help to increase in the built-in field, while the naturally formed graded buffer layer benefits for the carrier transport and collection. In addition the wide bandgap results in a blocking barrier to repel the holes from the defective interface area and then reduce retro-diffusion of the holes in the *n*-layer. Hence, the nc-Si:H *n*-layer significantly enhances V_{oc} of a-Si:H solar cell approximately 50 mV or 100 mV higher than those cells with a-Si:H *n*-layer or microcrystalline silicon *n*-layer, respectively.

Acknowledgment

This research is supported by the National High-tech R&D Program of China (No. 2011AA050503), National Natural Science Foundation of China (No. 61176060), Key Project of Natural Science Foundation of Tianjin (No. 12JCZDJC28300), the National Basic Research Program of China (Nos. 2011CBA00705, 2011CBA00706 and 2011CBA00707) and Major Science and Technology Support Project of Tianjin (No. 11TXSYGX22100). The author (G. Hou) thanks Prof. Dr. Qi Hua Fan from EECS, South Dakota State University and Prof. Xianbo Liao from Institute of Semiconductors, CAS for their helpful discussion.

References

[1] H. Tan, E. Psomadaki, O. Isabella, M. Fischer, P. Babal, R. Vasudevan, M. Zeman, A. Smets, Micro-textures for efficient light trapping and improved electrical performance in thin-film nanocrystalline silicon solar cells, Appl. Phys. Lett. 103 (2013) 173905-1–173905-5.
[2] B. Yan, G. Yue, L. Sivec, J. Yang, S.u. Guha, C. Jiang, Innovative dual function nc-SiO_x:H layer leading to $\eta > 16\%$ efficient multi-junction thin-film silicon solar cell, 99 (2011) 113512-1–113512-3.
[3] S. Kim, J. Chung, H. Lee, J. Park, Y. Heo, H. Lee, Remarkable progress in thin-film silicon solar cells using high-efficiency triple-junction technology, Sol. Energy Mater. Sol. Cells 119 (2013) 26–35.
[4] S. Michard, V. Balmes, M. Meier, A. Lambertz, T. Merdzhanova, F. Finger, Microcrystalline silicon absorber layers prepared at high deposition rates for thin-film tandem solar cells, EPJ Photovolt. 4 (2013) 45201-1–45201-6.
[5] K. Soderstrom, G. Bugnon, R. Biron, C. Pahud, F. Meillaud, F.-J. Haug, C. Ballif, Thin-film silicon triple-junction solar cell with 12.5% stable efficiency on innovative flat light-scattering substrate, J. Appl. Phys. 112 (2012) 114503-1–114503-4.
[6] Xi Chen, Baohua Jia, Yinan Zhang, M.i.n. Gu, Exceeding the limit of plasmonic light trapping in textured screen-printed solar cells using Al nanoparticles and wrinkle-like graphene sheets, Light: Sci. Appl. 2 (e92) (2013) 1–6.
[7] Hitoshi Sai, Kimihiko Saito, Nana Hozuki, Michio Kondo, Relationship between the cell thickness and the optimum period of textured back reflectors in thin-film microcrystalline silicon solar cells, Appl. Phys. Lett. 102 (2013) 053509-1–053509-5.
[8] C. Battaglia, J. Escarré, K. Soderstrom, M. Charrière, M. Despeisse, F.-J. Haug, C. Ballif, Nanomoulding of transparent zinc oxide electrodes for efficient light trapping in solar cells, Nat. Photonics 5 (2011) 535–538.
[9] A. Polman, H.A. Atwater, Photonic design principles for ultrahigh-efficiency photovoltaics, Nat. Mater. 11 (2012) 174–177.
[10] B. Yan, J. Yang, S. Guha, Effect of hydrogen dilution on the open-circuit voltage of hydrogenated amorphous silicon solar cells, Appl. Phys. Lett. 83 (2003) 782–784.
[11] W. Du, X. Liao, X. Yang, H. Povolny, X. Xiang, X. Deng, K.a.i. Sun, Hydrogenated nanocrystalline silicon p-layer in amorphous silicon n–i–p solar cells, Sol. Energy Mater. Sol. Cells 90 (2006) 1098–1104.
[12] I.A. Yunaz, S. Miyajima and M. Konagai, Silicon based multijunction solar cells with wide-gap a-$Si_{1-x}C_x$:H top cell: experimental and numerical approaches, in: Conference Record of the 35th IEEE Photovoltaic Specialists Conference, Honolulu, HI, USA, Jun. 2010, pp. 317–322.
[13] R.E.I. Schropp, J.A. Schüttauf, C.H.M. Van Der Werf, Oxygenated protocrystalline silicon thin films for wide bandgap solar cells, Mater. Res. Soc. Symp. Proc. 1245 (2010) (1245-A02-03).
[14] J. Ni, J. Zhang, Y. Cao, X. Wang, X. Chen, X. Geng, Y. Zhao, Low temperature deposition of high open-circuit voltage (> 1.0 V) p–i–n type amorphous silicon solar cells, Sol. Energy Mater. Sol. Cells 95 (2011) 1922–1926.
[15] Y. Matsumoto, F. MeleHndez, R. Asomoza, Performance of p-type silicon-oxide windows in amorphous silicon solar cell, Sol. Energy Mater. Sol. Cells 66 (2001) 163–170.
[16] S. Myong, H. Lee, E. Yoon, K. Lim, Highly conductive boron-doped nanocrystalline silicon-carbide film prepared by low-hydrogen-dilution photo-CVD method using ethylene as a carbon source, J. Non-Cryst. Solids 298 (2002) 131–136.
[17] R. Biron, C. Pahud, F.J. Haug, J. Escarre, K. Soderstrom, C. Ballif, Window layer with p doped silicon oxide for high V_{oc} thin-film silicon n–i–p solar cells, J. Appl. Phys. 110 (2011) 124511-1–124511-7.
[18] J.M. Pearce, R.J. Koval, A.S. Ferlauto, R.W. Collins, C.R. Wronski, J. Yang, S. Guha, Dependence of open-circuit voltage in hydrogenated protocrystalline silicon solar cells on carrier recombination in p/i interface and bulk regions, Appl. Phys. Lett. 77 (2000) 3093–3095.

[19] J. Lee, V. Dutta, J. Yoo, J. Yi, J. Song, K. Yoon, Superstrate p–i–n a-Si:H solar cells on textured ZnO:Al front transparent conduction oxide, Superlattices Microstruct. 42 (2007) 369–374.
[20] F. Haug, R. Biron, G. Kratzer, F. Leresche, J. Besuchet, C. Ballif, M. Dissel, S. Kretschmer, W. Soppe, P. Lippens, K. Leitner, Improvement of the open circuit voltage by modifying the transparent indium–tin oxide front electrode in amorphous n–i–p solar cells, Prog. Photovolt.: Res. Appl. 20 (2012) 727–734.
[21] Y. Poissant, P. Chatterjee, P. Roca i Cabarrocas, No benefit from microcrystalline silicon N layers in single junction amorphous silicon p–i–n solar cells, J. Appl. Phys. 93 (2003) 170–174.
[22] K. Soderstrom, F.-J. Haug, V. Terrazzoni-Daudrix, C. Ballif, Optimization of amorphous silicon thin film solar cells for flexible photovoltaics, J. Appl. Phys. 103 (2008) 114509-1–114509-8.
[23] J. Tauc, Amorphous and Liquid Semiconductors, Plenum, New York (1974) 1974159.
[24] S. Veprek, F.A. Sarott, Z. Iqbal, Effect of grain boundaries on the Raman spectra, optical absorption, and elastic light scattering in nanometer-sized crystalline silicon, Phys. Rev. B 36 (1987) 3344–3350.
[25] J. Zi, H. Büscher, C. Falter, W. Ludwig, K. Zhang, X. Xie, Raman shifts in Si nanocrystals, Appl. Phys. Lett. 69 (1996) 200–202.
[26] J. Tauc, R. Grigorovici, A. Vancu, Optical properties and electronic structure of amorphous germanium, Phys. Status Solidi B 15 (1966) 627–637.
[27] Basudeb Sain, Debajyoti Das, Development of nc-Si/a-SiN_x:H thin films for photovoltaic and light-emitting applications, Sci. Adv. Mater. 5 (2013) 1–11.
[28] V. Švrek, I. Pelant, J. Koka, P. Fojtk, B. Rezek, H. Stuchlková, A. Fejfar, J. Stuchlk, A. Poruba, J. Toušek, Transport anisotropy in microcrystalline silicon studied by measurement of ambipolar diffusion length, J. Appl. Phys. 89 (2001) 1800–1805.
[29] Fengzhen Liu, Meifang Zhu, Q.i. Wang, Anisotropic electronic transport in microcrystalline silicon thin films, Phys. Lett. A 331 (2004) 432–436.
[30] G. Hou, X. Han, X. Geng, X. Zhang, C. Wei, J. Sun, X. Chen, J. Zhang, Y. Zhao, Structural evolution optimization at p/i interface and in the bulk intrinsic-layer for high efficiency microcrystalline silicon solar cells, Phys. Status Solidi C 7 (2010) 1089–1092.
[31] B. Yan, C. Jiang, Y. Yan, L. Sivec, J. Yang, S. Guha, M.M. Al-Jassim, Effect of hydrogen dilution profiling on the microscopic structure of amorphous and nanocrystalline silicon mixed-phase solar cells, Phys. Status Solidi C 7 (2010) 513–516.
[32] Tae-Youb Kim, Nae-Man Park, Kyung-Hyun Kim, G.u.n. Yong Sung, Young-Woo Ok, Tae-Yeon Seong, Cheol-Jong Choi, Quantum confinement effect of silicon nanocrystals in situ grown in silicon nitride films, Appl. Phys. Lett. 85 (2004) 5355–5357.
[33] W.A. Su, W.Z. Shen, A statistical exploration of multiple exciton generation in silicon quantum dots and optoelectronic application, Appl. Phys. Lett. 100 (2012) 071111.
[34] Shoji Furukawa, Tatsuro Miyasato, Quantum size effects on the optical band gap of microcrystalline Si:H, Phys. Rev. B 38 (1988) 5726–5729.
[35] J. Müllerová, V. Vavrunková, P. Šutta, On nanometer ordering in thin amorphous hydrogenated silicon, Adv. Electr. Electron. Eng. 7 (2008) 369–372.